J|A|C|S ARTICLES

Published on Web 03/10/2010

Electron Hydration and Ion−Electron Pairs in Water Clusters Containing Trivalent Metal Ions

William A. Donald, Maria Demireva, Ryan D. Leib, M. Jeannette Aiken, and Evan R. Williams*

Department of Chemistry, University of California, Berkeley, California 94720-1460

Received September 17, 2009; E-mail: williams@cchem.berkeley.edu

Abstract: The hydrated electron is one of the most fundamental nucleophiles in aqueous solution, yet it is a transient species in liquid water, making it challenging to study. The solvation thermodynamics of the electron are important for determining the band structure and properties of water and aqueous solutions. However, a wide range of values for the electron solvation enthalpy (−1.0 to −1.8 eV) has been obtained from previous methods, primarily because of the large uncertainty as to the value for the absolute proton solvation enthalpy. In the gas phase, electron interactions with water can be investigated in stable water clusters that contain an excess electron, or an electron and a solvent-separated monovalent or divalent metal ion. Here, we report the generation of stable water clusters that contain an excess electron and a solvent-separated *trivalent* metal ion that are formed upon electron capture by hydrated trivalent lanthanide clusters. From the number of water molecules lost upon electron capture, adiabatic recombination energies are obtained for $La(H_2O)_n^{3+}$ ($n = 42-160$). The trend in recombination energies as a function of hydration extent is consistent with a structural transition from a surface-located excess electron at smaller sizes ($n \leq \sim 56$) to a more fully solvated electron at larger sizes ($n \geq \sim 60$). The recombination enthalpies for $n > 60$ are extrapolated as a function of the geometrical dependence on cluster size to infinite size to obtain the bulk hydration enthalpy of the electron (−1.3 eV). This extrapolation method has the advantages that it *does not* require estimates of the absolute proton or hydrogen hydration enthalpies.

Introduction

Information about the effects of solvent on ion structure and, conversely, how ions influence solvent organization is fundamental to understanding the molecular structure and stability of ions in solution. Ion−solvent interactions are important to the structural, thermodynamic, and dynamic characteristics of many chemical, biological, and atmospheric processes, such as charge transfer reactions, catalysis, radiolysis, and ion nucleation events. Ion−solvent interactions can be investigated in gaseous hydrated clusters as a function of hydration extent and content, including individual ions either with or without counterions. The range of ion−water interactions that can be studied has been greatly expanded by the introduction of methods to form water clusters containing divalent[1] and trivalent[2] metal ions, as well as those that contain solvent-separated ion pairs.[3] Information about the structures of such microhydrated ions has been obtained from a variety of thermochemical,[1,4,5] spectroscopic,[6,7] and computational approaches.[8,9] From these and other studies, detailed information about how water organizes around ions and how hydration affects the structures of the ions themselves can be obtained.[10,11] Information about how a finite number of water molecules can solvate and cause dissociation of ionic salt pairs,[8] as well as acids,[12] may also be deduced.

One of the most fundamental charged species is the electron, which in liquid water is ephemeral, owing to its high reactivity ($E°_{1/2} = -2.6$ to -2.9 V)[13] with trace impurities (the rate constants of e^-(aq) reacting with many different trace species found in water containing e^-(aq) is on the order of 10^9 or 10^{10} L mol^{-1} s^{-1}).[13] The kinetics, thermodynamics, and dynamic properties of the hydrated electron, which is likely in an s-like ground state orbital and is trapped in a cavity surrounded by water molecules,[14,15] have been previously investigated using an assortment of experimental and theoretical techniques,

(1) Jayaweera, P.; Blades, A.; Ikonomou, M.; Kebarle, P. *J. Am. Chem. Soc.* **1990**, *112*, 2452–2454.
(2) Bush, M. F.; Saykally, R. J.; Williams, E. R *Int. J. Mass Spectrom.* **2006**, *253*, 256–262.
(3) Hertel, I. V.; Huglin, C.; Nitsch, C.; Schulz, C. P. *Phys. Rev. Lett.* **1991**, *67*, 1767–1770.
(4) Rodriguez-Cruz, S. E.; Jockusch, R. A.; Williams, E. R. *J. Am. Chem. Soc.* **1998**, *120*, 5842–5843.
(5) Carl, D. R.; Moision, R. M.; Armentrout, P. B. *Int. J. Mass Spectrom.* **2007**, *265*, 308–325.
(6) Bush, M. F.; Saykally, R. J.; Williams, E. R. *Chem. Phys. Chem.* **2007**, *8*, 2245–2253.
(7) Bush, M. F.; Saykally, R. J.; Williams, E. R. *J. Am. Chem. Soc.* **2008**, *130*, 9122–9128.
(8) Siu, C.-K.; Fox-Beyer, B. S.; Beyer, M. K.; Bondybey, V. E. *Chem. Eur. J.* **2006**, *12*, 6382–6392.
(9) Reinhard, B. M.; Niedner-Schatteburg, G. *J. Chem. Phys.* **2003**, *118*, 3571–3582.
(10) Blom, M.; Compagnon, I.; Polfer, N.; von Helden, G.; Meijer, G.; Suhai, S.; Paizs, B.; Oomens, J. *J. Phys. Chem. A* **2007**, *111*, 7309–7316.
(11) Bush, M.; Prell, J.; Saykally, R.; Williams, E. *J. Am. Chem. Soc.* **2007**, *129*, 13544–13553.
(12) Gutberlet, A.; Schwaab, G.; Birer, O.; Masia, M.; Kaczmarek, A.; Forbert, H.; Havenith, M.; Marx, D. *Science* **2009**, *324*, 1545–1548.
(13) Buxton, G. V.; Greenstock, C. L.; Helman, W. P.; Ross, A. B. *J. Phys. Chem. Ref. Data Ser.* **1988**, *17*, 513–886.
(14) Kevan, L. *Acc. Chem. Res.* **1981**, *14*, 138–145.
(15) Rossky, P. J.; Schnitker, J. *J. Phys. Chem.* **1988**, *92*, 4277–4285.

including measurements of reaction kinetics from radiolysis studies,[16−21] electron spin resonance of an excess electron trapped in ice,[22] Raman spectroscopy,[23] and computations.[24]

The hydration enthalpy of the electron is one of the most important properties that characterizes the stability and reactivity of the hydrated electron. The absolute hydration enthalpy of the electron is the enthalpy difference between a hydrated electron in a pure aqueous solution and an electron at rest under vacuum at an infinite distance from bulk water. Three different pulse radiolysis methods have been used to investigate the stability of the hydrated electron by measuring the enthalpies of the reactions given in eqs 1,[18,25] 2,[19] and 3.[20]

$$H + OH^- \rightarrow e^- + H_2O \quad (1)$$

$$e^- + H^+ \rightarrow H \quad (2)$$

$$e^- + NH_4^+ \rightarrow H + NH_3 \quad (3)$$

From the enthalpy of any of these reactions and a corresponding Born−Haber type thermodynamic cycle, a value for the solvation enthalpy of the electron can be obtained. These cycles include the absolute solvation enthalpy of the proton, which is the enthalpy difference between a proton in water and a proton at rest under vacuum. However, obtaining an accurate value for the proton solvation enthalpy is challenging because, in solution, it is not possible to directly separate the thermodynamic contribution of a single ion from its counterion. Instead, ion solvation enthalpies of one ion relative to another ion are obtained from solution-phase redox and/or dissolution experimental data. This results in a ladder of relative thermodynamic values which is anchored to the value for the proton that is commonly assigned an arbitrary value of 0.

Much effort has been devoted toward establishing an absolute ion solvation thermodynamic scale. Values for the solvation enthalpy of the proton in liquid water ranging from −274.9 to −260.0 kcal/mol have been reported.[26−33] In combination with these proton solvation enthalpy values, values for the electron solvation enthalpy can be obtained from the three different pulse radiolysis methods. Han and Bartels[18] reported a value of −1.31 eV for the hydration enthalpy of the electron using the proton solvation enthalpy value recommended by Conway (−267 kcal/mol)[26] and other thermodynamic values. Shiraishi et al. reported a value of −301.6 kcal/mol referenced to that of the proton.[19] Schwarz reported a value of 66.3 kcal/mol for the formation enthalpy of the hydrated electron referenced to that of the hydrated proton.[20] Using the same proton solvation enthalpy[26] as that used by Han and Bartels[18] results in a range of values from −1.31 to −1.50 eV for the solvation enthalpy of the electron from these three[18−20] pulse radiolysis studies. Combining this range in values derived from the pulsed radiolysis methods[18−20] with the range of the proton solvation enthalpies that have been reported[26−33] results in a range from −1.0 to −1.8 eV for the solvation enthalpy of the electron. Because of the wide range in values and the uncertainty as to the value for the proton solvation enthalpy, it would be interesting to develop alternative methods to obtain these values.

The interaction of electrons with water can also be investigated by probing the structures, reactivities, and dynamics of stable water clusters that contain an excess electron, $(H_2O)_n^-$,[34−43] as well as investigating stable clusters that contain an excess electron and a metal ion: e.g., $M(H_2O)_n$ (M = Li,[44] Na,[3,45,46] Cs)[47] and $M(H_2O)_n^+$ (M = Mg,[9,48,49] Ca[50]). Other insights into the interactions of an excess electron with water have been obtained by investigating the charge transfer of an electron to solvent upon laser activation of $I^-(H_2O)_n$,[51,52] or from photoelectron spectroscopy of $Na^-(H_2O)_n$.[44] From these different cluster types, electron−water interactions can be investigated in a gamut of different hydrated environments from water clusters containing only the excess electron to water clusters containing an excess electron that is solvent-separated from a neutral atom, a monovalent metal ion, or a divalent metal ion. It is interesting to know how water organizes around the electron in these types of clusters. Neumark and co-workers reported

(16) Matheson, M. S.; Rabani, J. *J. Phys. Chem.* **1965**, *69*, 1324–1335.
(17) Hart, E. J.; Gordon, S.; Fielden, E. M. *J. Phys. Chem.* **1966**, *70*, 150–156.
(18) Han, P.; Bartels, D. M. *J. Phys. Chem.* **1990**, *94*, 7294–7299.
(19) Shiraishi, H.; Sunaryo, G. R.; Ishigure, K. *J. Phys. Chem.* **1994**, *98*, 5164–5173.
(20) Schwarz, H. A. *J. Phys. Chem.* **1991**, *95*, 6697–6701.
(21) Bartels, D. M.; Takahashi, K.; Cline, J. A.; Marin, T. W.; Jonah, C. D. *J. Phys. Chem. A* **2005**, *109*, 1299–1307.
(22) Schlick, S.; Narayana, P. A.; Kevan, L. *J. Chem. Phys.* **1976**, *64*, 3153–3160.
(23) Tauber, M.; Mathies, R. *J. Am. Chem. Soc.* **2003**, *125*, 1394–1402.
(24) Schnitker, J.; Rossky, P. J. *J. Chem. Phys.* **1987**, *86*, 3471–3485.
(25) Jortner, J.; Noyes, R. M. *J. Phys. Chem.* **1966**, *70*, 770–774.
(26) Conway, B. E.; Salomon, M. In *Chemical Physics of Ionic Solutions*; Conway, B. E., Barradas, R. G., Eds.; Wiley: New York, 1966.
(27) Rashin, A. A.; Honig, B. *J. Phys. Chem.* **1985**, *89*, 5588–5593.
(28) Halliwell, H. F.; Nyburg, S. C. *Trans. Faraday Soc.* **1963**, *59*, 1126–1140.
(29) Tissandier, M. D.; Cowen, K. A.; Feng, W. Y.; Gundlach, E.; Cohen, M. H.; Earhart, A. D.; Coe, J. V.; Tuttle, T. R., Jr. *J. Phys. Chem. A* **1998**, *102*, 7787–7794.
(30) Coe, J. V. *Int. Rev. Phys. Chem.* **2001**, *20*, 33–58.
(31) Marcus, Y. *J. Chem. Soc. Faraday Trans. 1* **1987**, *83*, 339–349.
(32) Friedman, H. L.; Krishnan, C. V. In *Water: A Comprehensive Treatise*; Franks, F., Ed.; Plenum: New York, 1973; Vol. 3, pp 1−118.
(33) Mejías, J. A.; Lago, S. *J. Chem. Phys.* **2000**, *113*, 7306–7316.
(34) Verlet, J. R. R.; Bragg, A. E.; Kammrath, A.; Cheshnovsky, O.; Neumark, D. M. *Science* **2005**, *307*, 93–96.
(35) Verlet, J. R. R.; Bragg, A. E.; Kammrath, A.; Cheshnovsky, O.; Neumark, D. M. *Science* **2005**, *310*, 1769b.
(36) Coe, J. V.; Lee, G. H.; Eaton, J. G.; Arnold, S. T.; Sarkas, H. W.; Bowen, K. H.; Ludewigt, C.; Haberland, H.; Worsnop, D. R. *J. Chem. Phys.* **1990**, *92*, 3980–3982.
(37) Turi, L.; Sheu, W.-S.; Rossky, P. *Science* **2005**, *309*, 914–917.
(38) Bragg, A. E.; Verlet, J. R. R.; Kammrath, A.; Cheshnovsky, O.; Neumark, D. M. *Science* **2004**, *306*, 669–671.
(39) Bragg, A.; Verlet, J.; Kammrath, A.; Cheshnovsky, O.; Neumark, D. *J. Am. Chem. Soc.* **2005**, *127*, 15283–15295.
(40) Paik, D. H.; Lee, I.-R.; Yang, D.-S.; Baskin, J. S.; Zewail, A. H. *Science* **2004**, *306*, 672–675.
(41) Asmis, K. R.; Santambrogio, G.; Zhou, J.; Garand, E.; Headrick, J.; Goebbert, D.; Johnson, M. A.; Neumark, D. M. *J. Chem. Phys.* **2007**, *126*, 191105.
(42) Barnett, R. N.; Landman, U.; Cleveland, C. L.; Jortner, J. *J. Chem. Phys.* **1988**, *88*, 4429–4447.
(43) Coe, J. V.; Williams, S. M.; Bowen, K. H. *Int. Rev. Phys. Chem.* **2008**, *27*, 27–51.
(44) Takasu, R.; Misaizu, F.; Hashimoto, K.; Fuke, K. *J. Phys. Chem. A* **1997**, *101*, 3078–3087.
(45) Steinbach, C.; Buck, U. *J. Phys. Chem. A* **2006**, *110*, 3128–3131.
(46) Gao, B.; Liu, Z.-F. *J. Chem. Phys.* **2007**, *126*, 084501.
(47) Misaizu, F.; Tsukamoto, K.; Sanekata, M.; Fuke, K. *Chem. Phys. Lett.* **1992**, *188*, 241–246.
(48) Berg, C.; Beyer, M.; Achatz, U.; Joos, S.; Niedner-Schatteburg, G.; Bondybey, V. E. *Chem. Phys.* **1998**, *239*, 379–392.
(49) Reinhard, B. M.; Niedner-Schatteburg, G. *Phys. Chem. Chem. Phys.* **2002**, *4*, 1471–1477.
(50) Sanekata, M.; Misaizu, F.; Fuke, K.; Iwata, S.; Hashimoto, K. *J. Am. Chem. Soc.* **1995**, *117*, 747–754.
(51) Serxner, D.; Dessent, C. E. H.; Johnson, M. A. *J. Chem. Phys.* **1996**, *105*, 7231–7234.
(52) Verlet, J. R. R.; Kammrath, A.; Griffin, G. B.; Neumark, D. M. *J. Chem. Phys.* **2005**, *123*, 231102.

that at least three different $(H_2O)_n^-$ isomers were formed using a supersonic expansion cluster source based on the measured vertical detachment energies (VDEs) of these clusters for n up to ~150.[34] One of these isomers is reported to have an internally solvated electron based on the comparison of the measured VDEs with calculated values.[34,35] However, the location of the excess electron in the clusters has been the subject of intense debate, and evidence supporting both internally and externally solvated electrons has been reported.[34−43]

An alternative and unorthodox approach to probe the interactions of metal ions, electrons, and water is to investigate the thermodynamics of ion solvation by measuring the recombination energies (REs) resulting from electron capture (EC) by nanometer-sized hydrated metal ions.[53−63] In this method, termed hydrated metal ion nanocalorimetry, a gaseous droplet containing a multiply charged metal ion is reduced by a thermally generated electron. The reduction energy results in rapid heating of the cluster and evaporation of water molecules which reduces the cluster temperature to that of the initial cluster. The energy removed from the cluster by evaporative cooling is equal to the adiabatic recombination energy of the precursor cluster, because the rate of water reorganization is much faster than the time scale of the experiment and the water reorganization energy is reflected in the overall extent of water evaporation from the reduced nanodrop. The recombination energies are obtained from the average number of water molecules lost from the cluster, the sum of the threshold water molecule binding energies, and the energy that is partitioned into the translational, rotational, and vibrational modes of the products.[53,54] This technique has been used to obtain a value for the absolute standard hydrogen electrode potential from three different nanocalorimetry-based methods that all agree within 5% of each other (+4.05, +4.11, and +4.21 V).[53,55,56]

Upon EC, the electron is not necessarily captured by the individual cluster constituent that has the highest ionization energy in isolation. For example, reduction of $Ca(H_2O)_n^{2+}$ (n > 22) results in the formation of an ion−electron pair.[57−59] The trend in the REs with increasing cluster size for $Ca(H_2O)_n^{2+}$ (n up to 62) is consistent with a transition from a surface-located electron to a more solvated electron at $n \approx 47$.[57] Interestingly, Neumark and co-workers interpret the trend in the VDEs of $(H_2O)_n^-$, for the isomers that have the highest VDEs, as having a transition from a surface to an internally bound electron with increasing size for n between 12 and 25;[34,35] time-resolved photoelectron data also appear consistent with this transition to a bulk-like electron at n > ~25.[39] It is interesting to consider that the presence of the metal ion "pushes" the electron out of the cluster and results in a transition that occurs at a larger hydration extent vs that for $(H_2O)_n^-$, likely the result of steric and increased water patterning effects caused by the presence of the divalent metal ion. However, such comparisons should be made with caution because of the different conditions under which these two cluster types are generated and uncertainty as to the location of the electron in $(H_2O)_n^-$.

Here, we report evidence that large water clusters containing an excess electron and a *trivalent* metal ion can be formed and are stable in the gas phase. The effects of size and ion identity on the reactivity of these nanodrops have been investigated. The trend in the REs for $La(H_2O)_n^{3+}$, for n from 42 to 160, is consistent with a transition from a surface-located excess electron to a more fully solvated electron at $n \approx 58$. The REs for n > 60 are extrapolated to infinite cluster size to obtain a value for the bulk solvation enthalpy of the electron. This value is consistent with the wide range of previous values, but our method has the advantage that an estimate of the absolute proton solvation enthalpy, which is the primary source of uncertainty with prior methods, is unnecessary.

Experimental Section

All experiments were performed on the Berkeley 2.75 T Fourier transform ion cyclotron resonance mass spectrometer equipped with an external nanoelectrospray ion source and an ion cell surrounded by a temperature-controllable copper jacket that is equilibrated to 133 K.[2,59,64] Extensively hydrated ions are formed by nanoelectrospray from ~5 mM aqueous solutions of metal(III) chloride or nitrate salts. A positive potential of ~500−800 V relative to the heated capillary (~75−100 °C) entrance of the mass spectrometer is applied to a Pt wire that is in direct contact with the metal(III) salt solution. This solution is contained in a borosilicate capillary that has an inner tip diameter of ~2 μm. Ions are introduced into the cell of the mass spectrometer through five stages of differential pumping and are accumulated in the cell for 2.7−8.0 s, during which time N_2(g) is pulsed into the cell chamber to pressures of $\sim 1 \times 10^{-6}$ Torr to enhance trapping and thermalization of the ions. A mechanical shutter is subsequently closed to prevent additional ions from entering the cell. Ions are stored for an additional ~3.0−9.0 s so that the ion cell pressure returns to $\leq 10^{-8}$ Torr and to ensure that the ions have steady-state internal energy distributions at the temperature of the copper jacket surrounding the ion cell (133 K).

For electron capture dissociation experiments,[59] ions of interest are isolated using SWIFT waveforms. Following a 40 ms delay, electrons generated from a heated dispensor cathode located axially 20 cm from the cell center are introduced into the cell by applying −1.5 V for 120 ms to the cathode housing. A delay ranging from 40 ms to 1.5 s between the end of electron irradiation and ion excitation/detection is used to ensure that dissociation of the reduced precursor is complete. A +10 V potential is applied to the cathode at all other times to prevent electrons from entering the cell. A potential of +9 V is applied to a Cu wire mesh mounted 0.5 cm in front of the cathode.

The average number of water molecules lost from the reduced precursor is obtained from a weighted average of the observed product ion intensities and is corrected for the loss of water molecules resulting from the absorption of blackbody photons that occurs in the absence of EC to give the average number of water molecules lost due to EC alone. Average internal energies are calculated as described previously[53,54] using calculated harmonic frequencies for an energy-minimized B3LYP/LACVP**++ struc-

(53) Donald, W. A.; Leib, R. D.; O'Brien, J. T.; Bush, M. F.; Williams, E. R. *J. Am. Chem. Soc.* **2008**, *130*, 3371–3381.
(54) Donald, W. A.; Williams, E. R. *J. Am. Soc. Mass Spectrom.* 2009. doi: 10.1016/j.jasms.2009.12.006.
(55) Donald, W. A.; Leib, R. D.; Demireva, M.; O'Brien, J. T.; Prell, J. S.; Williams, E. R. *J. Am. Chem. Soc.* **2009**, *131*, 13328–13337.
(56) Donald, W. A.; Leib, R. D.; O'Brien, J. T.; Williams, E. R. *Chem. Eur. J.* **2009**, *15*, 5926–5934.
(57) Donald, W. A.; Leib, R. D.; O'Brien, J. T.; Holm, A. I. S.; Williams, E. R. *Proc. Natl. Acad. Sci. U.S.A.* **2008**, *105*, 18102–18107.
(58) Leib, R. D.; Donald, W. A.; Bush, M. F.; O'Brien, J. T.; Williams, E. R. *J. Am. Chem. Soc.* **2007**, *129*, 4894–4895.
(59) Leib, R. D.; Donald, W. A.; Bush, M. F.; O'Brien, J. T.; Williams, E. R. *J. Am. Soc. Mass Spectrom.* **2007**, *18*, 1217–1231.
(60) Leib, R. D.; Donald, W. A.; O'Brien, J. T.; Bush, M. F.; Williams, E. R. *J. Am. Chem. Soc.* **2007**, *129*, 7716–7717.
(61) O'Brien, J. T.; Prell, J. S.; Holm, A. I. S.; Williams, E. R. *J. Am. Soc. Mass Spectrom.* **2008**, *19*, 772–779.
(62) Prell, J. S.; O'Brien, J. T.; Holm, A. I. S.; Leib, R. D.; Donald, W. A.; Williams, E. R. *J. Am. Chem. Soc.* **2008**, *130*, 12680–12689.
(63) Holm, A. I. S.; Donald, W. A.; Hvelplund, P.; Larsen, M. K.; Nielsen, S. B.; Williams, E. R. *J. Phys. Chem. A* **2008**, *112*, 10721–10727.
(64) Wong, R. L.; Paech, K.; Williams, E. R. *Int. J. Mass Spectrom.* **2004**, *232*, 59–66.

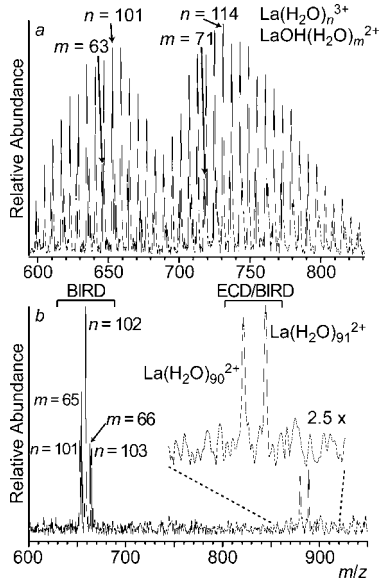

Figure 1. (a) Nanoelectrospray ionization mass spectrum of an aqueous $LaCl_3$ solution showing distributions of $La(H_2O)_n^{3+}$ and $LaOH(H_2O)_m^{2+}$ and (b) electron capture dissociation (ECD) mass spectrum of isolated $La(H_2O)_{103}^{3+}$ resulting in the loss of 12 and 13 water molecules from the reduced precursor as a result of ECD and blackbody infrared radiative dissociation (BIRD). The inset gives a 2.5× vertical expansion of the mass spectrum for *m*/*z* 850−920.

ture for $Ca^{2+}(H_2O)_{14}$. For larger clusters, average internal energies are obtained by scaling the vibrational degrees of freedom of $Ca(H_2O)_{14}^{2+}$ by the vibrational degrees of freedom of the larger cluster.

Molecular mechanics simulations of $Mo^{3+}I^-(H_2O)_n$ were performed using the OPLS-2005 force field implemented in MacroModel 8.1 (Schrödinger, Inc., Portland, OR) at 300 K and with no electrostatic cutoffs. Five starting structures were generated by fixing the Mo^{3+}/I^- bond distance (*d*) at ∼2.6 Å, which corresponds to the equilibrium bond distance for this ionic pair in isolation, adding the appropriate number of water molecules randomly around the ion pair core, running the simulation at a temperature of 300 K, and sampling one structure every 200 ps. These five starting structures were then run under the same conditions, except that the Mo^{3+} and I^- were allowed to move relative to each other and structures were recorded every 10 ps.

Results and Discussion

Electron Capture by Thermal Size-Selected $M(H_2O)_n^{3+}$. Nanoelectrospray ionization of aqueous solutions containing ∼5 mM $LaCl_3$ results in the formation of wide distributions of $La(H_2O)_n^{3+}$ and $LaOH(H_2O)_m^{2+}$ ($n = 92-130$ and $m = 58-83$; Figure 1a) that are thermalized to the temperature of the copper jacket surrounding the ion cell (133 K). The range of cluster sizes can be shifted to larger or smaller sizes by changing instrumental parameters, such as the temperature of the capillary in the electrospray ionization interface. Results for EC by $La(H_2O)_{103}^{3+}$ are shown in Figure 1b. The loss of 12 and 13 water molecules from the reduced precursor is observed. A delay of 1.0 s after EC and prior to ion detection is used to ensure that dissociation due to EC is complete. During this delay, substantial loss of water from $La(H_2O)_{103}^{3+}$ occurs, owing to the absorption of photons from the surrounding blackbody field.[65] The average number of water molecules lost due to EC alone is obtained by correcting the average water molecule loss from the reduced precursor as a result of EC and blackbody infrared radiative dissociation (BIRD) (12.4 water molecules) for the average number of water molecules lost due to BIRD alone. This latter value is estimated from the average number of water molecules lost from the precursor without electrons injected into the cell (0.9 water molecule). Thus, the average number of water molecules lost due to EC alone is 12.4 − 0.9 = 11.5 water molecules for this ion. The width of the product ion distribution is remarkably narrow compared to the number of water molecules that are lost.

Effects of Size and Charge State on Electron Capture Fragmentation Pathways. In addition to the reduced cluster dissociating via sequential water molecule loss, clusters can dissociate via the loss of a hydrogen atom and water molecules to form a hydrated metal hydroxide cluster.[56,59] These two competitive dissociation pathways are shown in Scheme 1.

Scheme 1

$$M(H_2O)_n^{z+} + e^- \xrightarrow{\text{I}} M(H_2O)_{n-x}^{(z-1)+} + x(H_2O)$$
$$\xrightarrow{\text{II}} MOH(H_2O)_{n-y-1}^{(z-1)+} + y(H_2O) + H$$

The branching ratio between these two processes depends upon the precursor cluster size and the metal ion identity (Figure 2). For $La(H_2O)_n^{3+}$, pathway II dissociation occurs exclusively for $n \leq 39$, whereas pathway I dissociation occurs exclusively for $n \geq 52$. The transition between pathway I and II dissociation for $La(H_2O)_n^{3+}$ occurs over a slightly wider range in cluster sizes and at significantly larger cluster sizes ($n = 39-52$) than for $Ca(H_2O)_n^{2+}$ ($n = 22-30$).[59] These data are consistent with previous results for the alkaline-earth-metal ions[56] that indicate dissociation via H atom loss is favored for metal ions with higher charge densities and for smaller cluster sizes. For a single size selected $La(H_2O)_n^{3+}$ cluster that dissociates via both pathways ($n = 42-48$), the average numbers of water molecules lost (between 12 and 13) via each pathway are comparable, which indicates that loss of a H atom from $La(H_2O)_n^{2+}$ ($n < \sim 42 - 12 = \sim 30$) occurs readily under these conditions. Possible mechanisms for H atom loss upon EC are discussed elsewhere.[57,66]

Dissociation Time Scale. For the smaller clusters investigated, dissociation upon EC is very rapid relative to the time scale of the experiments.[59] However, for the larger clusters, the effective temperature of the reduced cluster decreases with increasing

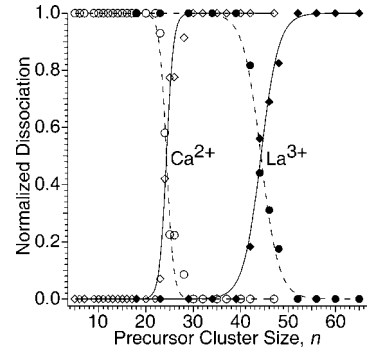

Figure 2. Normalized product ion intensities for dissociation by pathway I (loss of water molecules, diamonds) and pathway II (loss of H and water molecules, circles) resulting from electron capture by $Ca(H_2O)_n^{2+}$ (open symbols) or $La(H_2O)_n^{3+}$ (closed symbols). Rapid transitions between each pathway occur at $n = 22-30$ for $Ca(H_2O)_n^{2+}$ and $n = 39-52$ for $La(H_2O)_n^{3+}$. The data for Ca have been published previously.[59] Sigmoidal trend lines were fit to these data as a guide.

(65) Price, W. D.; Schnier, P. D.; Williams, E. R. *Anal. Chem.* **1996**, *68*, 859–866.

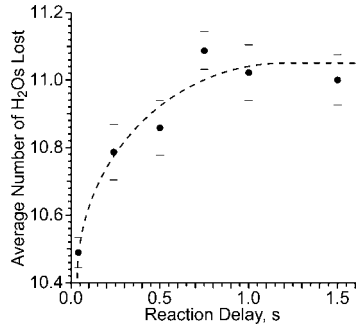

Figure 3. Average number of water molecules lost from $La(H_2O)_{125}^{3+}$ as a result of EC as a function of the reaction time delay between the end of EC and ion detection. The dashed line is a guide for the eye. Error bars are propagated from 1 standard deviation in the noise level in the mass spectra.

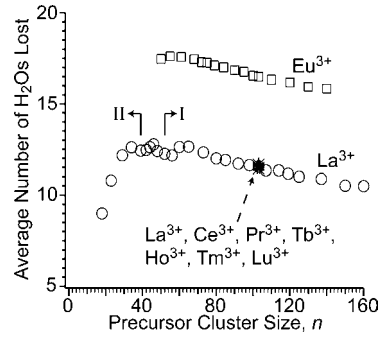

Figure 4. Average number of water molecules lost as a result of EC alone (data corrected for loss by BIRD) as a function of the precursor cluster size for $M(H_2O)_n^{3+}$ (M = La, Eu) and $M(H_2O)_{103}^{3+}$ (M = Ce, Pr, Tb, Ho, Tm, Lu). Solid arrows indicate precursor cluster sizes in which pathway I or II is exclusively observed for hydrated La^{3+}. The data for Eu have been published previously.[55]

cluster size, owing to two factors: the RE decreases with increasing size due to increased ion solvation by additional water molecules[53,55,57] and the RE is distributed over more degrees of freedom with increasing cluster size. These two factors result in a slower rate of water evaporation upon EC with increasing cluster size. Thus, for the larger clusters, it is important to ensure that water evaporation is complete prior to ion detection to obtain accurate RE values. Radiative and collisional cooling effects are expected to be minor under the conditions of these experiments.

To investigate the rate of water evaporation from the clusters activated via EC, a variable reaction time delay between the end of EC and beginning of ion detection was used for experiments with isolated $La(H_2O)_{65}^{3+}$, $La(H_2O)_{125}^{3+}$, and $La(H_2O)_{160}^{3+}$. For $n = 65$, an average of 12.59 water molecules are lost due to EC only for a reaction time delay of 40 ms, whereas a delay of 0.5 s results in an average of 12.67 water molecules lost. This indicates that, for this size cluster and smaller, the reaction is rapid. For $n = 125$, the average number of water molecules due to EC are plotted as a function of the reaction time delay for times ranging from 40 ms to 1.5 s in Figure 3. The average number of water molecules lost increases from 10.5 at 40 ms to ~11.0 at 1.0 s and longer. These data indicate that the reaction is complete somewhere between 500 and 750 ms. For $n = 160$, a delay of 1.0 s results in an average of 10.49 water molecules lost, whereas a 1.5 s delay results in 10.40 water molecules. This indicates that 1.0 s is a sufficiently long reaction time. For all $n \leq 65$, a delay of 40 ms is used, for $65 < n < 125$ a delay of 1.0 s is used, and for $n \geq 125$, a delay of 1.5 s is used to ensure that the reaction is complete for each cluster size investigated.

Effects of Cluster Size and Ion Identity on the Extent of Water Molecule Loss. The average numbers of water molecules lost upon EC by $M(H_2O)_n^{3+}$ (M = La, Eu) and by $M(H_2O)_{103}^{3+}$ (M = Ce, Pr, Tb, Ho, Tm, Lu) are shown in Figure 4. At the smaller cluster sizes, the extent of water molecule loss decreases with decreasing cluster size because both the water molecule binding energies and the energy that partitions into the products upon water molecule loss increase with decreasing cluster size. For example, $La(H_2O)_{34}^{3+}$ loses an average of 12.7 water molecules as a result of EC, whereas $La(H_2O)_{18}^{3+}$ loses 9.0 water molecules. As the cluster size increases, the average number of water molecules lost reaches a plateau and then decreases with increasing cluster sizes. The decrease in the average number of water molecules lost with increasing size is predominantly due to ion solvation that increases with increasing cluster size. The plateau at intermediary cluster sizes is a result of competition between ion solvation effects and effects of water molecule binding energies and energy partitioning into the translational and rotational modes of the products.

Metal ion identity can strongly affect the extent of water molecule loss from the nanodrops as a result of electron capture. For example, the average number of water molecules lost from $Eu(H_2O)_{103}^{3+}$ (16.0 water molecules)[55] is much greater than that for $M(H_2O)_{103}^{3+}$ (M = La, Ce, Pr, Tb, Ho, Tm, Lu), which all lose nearly the same average number of water molecules as a result of EC (between 11.5 and 11.7 water molecules), despite the differences in the third ionization energies of the unsolvated metal atoms that range from 19.18 eV for La to 23.68 eV for Tm.[67] Because the clusters containing trivalent La, Ce, Pr, Tb, Ho, Tm, and Lu lose nearly the same number of water molecules and because many other trivalent metal ion containing water clusters (e.g., Eu^{3+}, $M(NH_3)_6^{3+}$ (M = Ru, Co, Os, Cr, Ir))[53] lose both *different* numbers of water molecules (between 14 and 19) and *more* water molecules (up to ~5.6 more water molecules for $Ru(NH_3)_6(H_2O)_{55}^{3+}$ [53] than for $La(H_2O)_{60}^{3+}$), these data indicate that EC by $M(H_2O)_n^{3+}$ (M = La, Ce, Pr, Tb, Ho, Tm, Lu) results in the formation of a solvent-separated ion−electron pair at sizes in which dissociation via pathway I occurs ($n \geq 42$, for $La(H_2O)_n^{3+}$). These results are entirely consistent with the fact that, in aqueous solution, one-electron reduction of M^{3+} = La, Ce, Pr, Tb, Ho, Tm, Lu, does not occur, whereas the one-electron-reduction potentials of Eu^{3+} and $M(NH_3)_6^{3+}$ (M = Ru, Co, Cr, Os, Ir) are readily measurable. Thus, the EC reactivity of these hydrated metal ions correlates with the bulk solution-phase redox chemistry.

Adiabatic Recombination Energies from Experimental Cluster Measurements. Unlike many gas-phase methods used to determine ionization energies, ion nanocalorimetry measurements can be used to obtain adiabatic recombination energy values because the solvent reorganization time (in the low picoseconds) is much faster than the time scale of the experiment. Adiabatic recombination energy values are obtained from the average number of water molecules lost from the reduced precursors, the sum of the threshold binding energies (E_0) for each lost water molecule, and the energy that partitions into

(66) Neff, D.; Simons, J. *Int. J. Mass Spectrom.* **2008**, *277*, 166–174.

(67) *CRC Handbook of Chemistry and Physics, Internet Version*; Lide, D. R., Ed.; Taylor and Francis: Boca Raton, FL, 2007.

Scheme 2

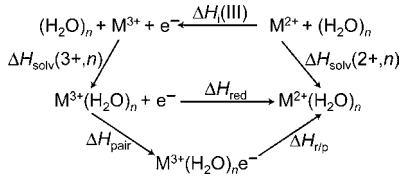

the translational, rotational, and vibrational energy of the products.[54] Briefly, threshold water molecule binding energies are obtained from the Thomson liquid drop model,[68,69] and the energy that partitions into the translational and rotational modes of the products upon sequential water molecule loss from the reduced clusters is obtained from a statistical model.[70] A detailed description of this method for obtaining RE values from the average number of water molecules lost is given elsewhere.[54]

Ion−Electron Pairing versus Reduction. It is remarkable that a *trivalent* metal ion and electron can be separated in a small nanocluster. To better understand the competition between direct metal ion reduction and formation of a solvent-separated ion−electron pair upon EC by $M(H_2O)_n^{3+}$, the thermodynamic cycles shown in Scheme 2 are useful, where $\Delta H_i(III)$ is the third ionization enthalpy of a metal atom M, $\Delta H_{solv}(3+,n)$ and $\Delta H_{solv}(2+,n)$ correspond to the adiabatic enthalpy of solvating isolated M^{3+} or M^{2+}, respectively, in a cluster of n water molecules, ΔH_{red} and ΔH_{pair} are the recombination enthalpies for either direct metal ion reduction or formation of an ion−electron pair, respectively, and $\Delta H_{r/p}$ is the energy corresponding to direct metal reduction by the excess electron in a water cluster containing a solvent-separated ion−electron pair, $M^{3+}(H_2O)_ne^-$. From these thermodynamic cycles, the enthalpy that drives direct metal ion reduction, $\Delta H_{r/p}$, can be separated into the individual processes that contribute to this quantity (eq 4).

$$\Delta H_{r/p} = \Delta H_{red} - \Delta H_{pair} = -\Delta H_{pair} - \Delta H_i(III) - \Delta H_{solv}(3+,n) + \Delta H_{solv}(2+,n) \quad (4)$$

From eq 4, ion−electron pair formation will be favored for more negative values of $\Delta H_{solv}(3+,n)$ (i.e., for more stable hydrated M^{3+}), smaller values for $\Delta H_i(III)$, and less negative values of $\Delta H_{solv}(2+,n)$ (i.e., for less stable hydrated M^{2+}). ΔH_{pair} depends on ion charge state, but at a sufficiently large cluster size, it does not depend significantly on metal ion identity. Thus, metal ion reduction of the larger clusters is driven by the $\Delta H_i(III)$ value of the bare ion and the difference in the solvation energies of the divalent versus trivalent ion. Formation of a solvent-separated ion−electron pair upon EC of $M^{3+}(H_2O)_n$ (M = La, Ce, Pr, Tb, Ho, Tm, Lu) occurs because the corresponding third ionization energy of the bare metal is not great enough to overcome the change in ion solvation energy that would result if the metal ion was reduced in the nanodrop. This is consistent with the fact that Eu, which is directly reduced in the nanodrop, has a higher third ionization energy (24.9 eV)[67] than the other lanthanides investigated, which have third ionization energies that range from 19.2 to 23.7 eV.[67]

Molecular Dynamics Simulation of Ion Separation in Water Clusters. To investigate the effects of solvent on the interactions between a trivalent metal ion and an excess electron in aqueous nanodrops, OPLS-2005 molecular dynamics (MD) simulations were performed on water clusters containing Mo^{3+} and I^- with up to 160 water molecules (Figure 5). I^- has an effective ionic radius (2.2 Å)[71] that is comparable to the radius (2.1 Å) of the octahedral water cavity that has been suggested to trap the hydrated electron in ice,[22,72] and it has been used by others as an analogue for the hydrated electron in MD simulations.[73] Mo^{3+} is used because it is the largest trivalent metal that is parametrized for the software package used to perform these molecular mechanics calculations.

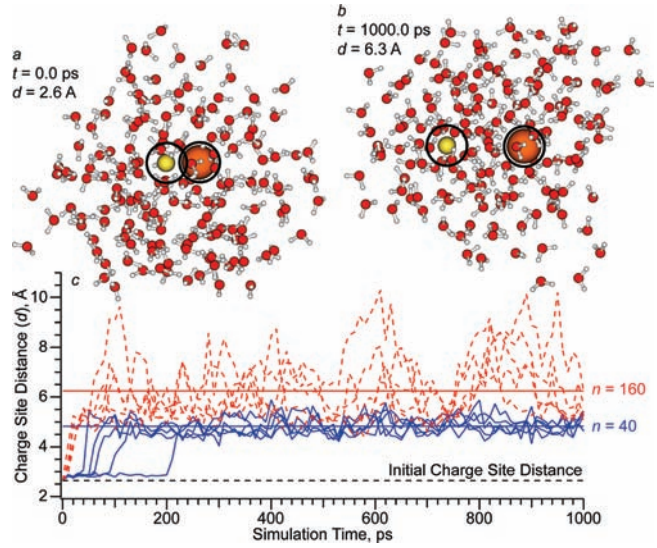

Figure 5. (a) $Mo^{3+}I^-(H_2O)_{160}$ structure obtained by fixing the Mo^{3+}/I^- distance at 2.6 Å (the equilibrium bond distance for this ion pair in isolation) in a cluster of 160 water molecules and running a molecular dynamics simulation for 1000 ps using an OPLS 2005 force field at 300 K. (b) Structure of $Mo^{3+}(H_2O)_nI^-$ obtained by running a molecular dynamics simulation for 1000 ps using an OPLS 2005 force field (300 K) starting with the structure shown in (a) and allowing the Mo^{3+}/I^- distance to vary freely. Mo^{3+} (yellow sphere) and I^- (orange sphere) are marked with black circles. (c) Center-to-center distance between Mo^{3+} and I^- as a function of simulation time for five different simulations starting from five different starting cluster structures resembling that in (a) for $n = 160$ (red dashed lines) or $n = 40$ (solid blue lines).

A representative starting structure for $Mo^{3+}I^-(H_2O)_{160}$ is shown in Figure 5a. After 1000 ps simulation, the structure in Figure 5b is obtained and is typical of the structures that are sampled in these simulations. The ion-to-ion distance is plotted as a function of simulation time in Figure 5c for two different cluster sizes ($n = 40$ and 160). After 10 to 200 ps, the ionic pair core of the nanodrop separates to form a solvent-separated ion pair, in which the iodide is usually at the surface (for $n < \sim100$) or within a solvent shell from the surface of the nanodrop ($n > \sim100$). The ions separate to an average ion-to-ion bond distance, $\langle d \rangle$, that depends on the number of water molecules in the cluster. For $n = 40$, the ions separate to an equilibrium distance of 4.8 ± 0.3 Å, whereas for $n = 160$, this distance is 6.2 ± 1.1 Å. For the latter cluster, nearly the same distance is obtained by running the simulation for 3 times as long (3 ns). Simulations in which I^- starts on the outside of a Mo^{3+}-containing cluster result in the same average ion-to-ion bond

(68) Holland, P. M.; Castleman, A. W., Jr. *J. Phys. Chem.* **1982**, *86*, 4181–4188.
(69) Donald, W. A.; Williams, E. R. *J. Phys. Chem. A* **2008**, *112*, 3515–3522.
(70) Klots, C. E. *J. Chem. Phys.* **1985**, *83*, 5854–5860.
(71) Shannon, R. D. *Acta Crystallogr.* **1976**, *A32*, 751–767.
(72) Feng, D.-F.; Kevan, L. *Chem. Rev.* **1980**, *80*, 1–20.
(73) Frigato, T.; VandeVondele, J.; Schmidt, B.; Schutte, C.; Jungwirth, P. *J. Phys. Chem. A* **2008**, *112*, 6125–6133.

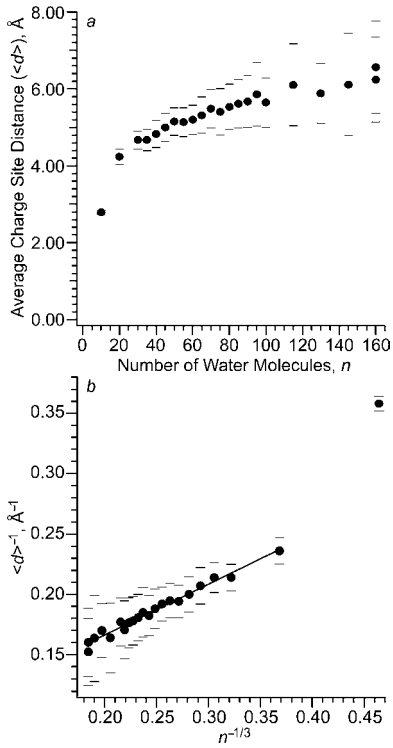

Figure 6. (a) Average distance between Mo^{3+} and I^- ($\langle d \rangle$) obtained from OPLS-2005 dynamics simulations at 300 K for $Mo^{3+}I^-(H_2O)_n$ as a function of n and (b) these same data plotted as $\langle d \rangle^{-1}$ (which is proportional to the electrostatic energy between the ions) versus $n^{-1/3}$ (which is proportional to the cluster radii). The error bars represent 1 standard deviation in the average distance of each structure monitored every 10 ps for ~4.8 ns for each cluster size. One nanosecond simulations were run using five different starting structures with an initial ion−ion bond distance of ~2.6 Å for each cluster. For n = 115, 130, 160, a 5 ns simulation using a single starting structure was used.

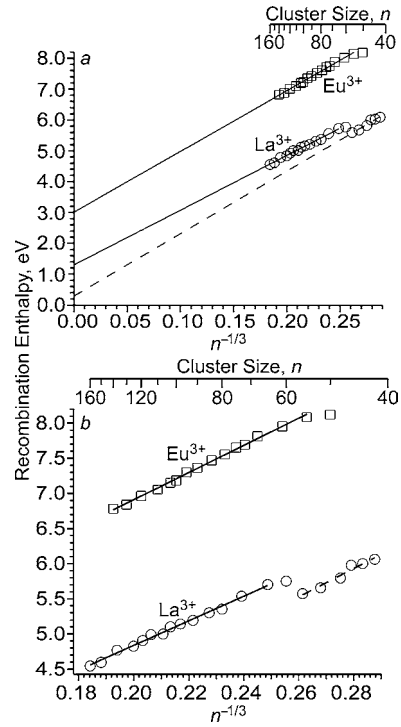

Figure 7. Recombination enthalpies of $Eu(H_2O)_n^{3+}$ (squares)[55] and $La(H_2O)_n^{3+}$ (circles) as a function of $n^{-1/3}$ with (a) the y axis intercept shown and (b) a magnified view shown. Solid black lines are linear regression best-fit lines to the EC data for either $Eu(H_2O)_n^{3+}$ (n = 55−140)[55] or $La(H_2O)_n^{3+}$ (n = 65−160). The dashed line is a linear regression best-fit line to EC data for $La(H_2O)_n^{3+}$ (n = 42−56). The data for Eu have been published previously.[55]

distance for a given sized cluster. These results indicate that 1000 ps simulation times at 300 K are adequate for the ion-to-ion bond distance to approach its equilibrium value.

Values for $\langle d \rangle$ were obtained as a function of cluster size for n from between 10 and 160 and are shown in Figure 6. The values of $\langle d \rangle$ range from 2.8 to 6.2 Å and generally increase smoothly with increasing cluster size (Figure 6a). The large change in $\langle d \rangle$ that occurs between n = 10 (2.8 Å) and 20 (4.2 Å) is due to the transition between a contact ion pair equilibrium set of structures for the former to solvent-separated ion pair equilibrium structures for the latter. With increasing cluster size, the fluctuations in d increase due to reduced electrostatic interaction between the ions and the increasing conformational space.

On the basis of Coulomb's law, a plot of $\langle d \rangle^{-1}$ versus $n^{-1/3}$ should result in a linear relationship if the structures of the clusters do not dramatically change as a function of cluster size and the ions do not interact significantly at infinite dilution (see the Supporting Information). Values for $\langle d \rangle^{-1}$, obtained from the cluster simulations, are plotted as a function of $n^{-1/3}$ in Figure 6b. A linear regression analysis of the simulation data for n = 20−160 results in a best-fit line with an R^2 value of 0.97, indicating that the simulation data agree well with the $n^{-1/3}$ relationship. The n = 10 data point is a significant outlier because the simulations for this cluster resulted in only contact ion pair structures after 1000 ps. The intercept corresponds to an inter-ion separation of 12.3 Å at infinite dilution. At this distance, the Coulomb attraction between the ion and electron is on the order of *RT*. Although the interaction between the ion and electron is not adequately modeled by these molecular dynamics simulations, these results do suggest that the Coulomb attraction between the ion and electron is sufficiently small that these ions will drift apart at infinite dilution. These results indicate that the $n^{-1/3}$ relationship applies to cases in which an ion−electron pair is formed in the nanodrops. This is consistent with calculations that indicate vertical ionization energies for hydrated clusters containing either a surface-bound or an interior electron should proceed as a linear function of $n^{-1/3}$.[74]

Extrapolation of Cluster Adiabatic Ionization Enthalpies to Bulk Water. To connect the cluster recombination energies to the corresponding electron solvation process in aqueous solution and investigate the structure of the La^{3+}-containing nanodrops, the recombination enthalpies are plotted as a function of the geometric dependence of these data on cluster size and extrapolated to an infinitely large cluster size.[55,57] Recombination enthalpy values for $La(H_2O)_n^{3+}$ and $Eu(H_2O)_n^{3+}$ are plotted as a function of $n^{-1/3}$ in Figure 7 for clusters that dissociate via pathway I.

The recombination enthalpy values for $La(H_2O)_n^{3+}$ linearly and monotonically decrease with increasing size for n = 42−56, but remarkably, the recombination enthalpy for n = 60 is significantly *larger* than that for n = 56. For n = 60−160, the recombination enthalpy values again decrease linearly and monotonically with increasing cluster size. To the extent that similar ion−electron pair structures are formed in the droplets upon EC, the recombination enthalpy values should depend linearly on $n^{-1/3}$. The origin of this break at n = ~58 can be

(74) Makov, G.; Nitzan, A. *J. Phys. Chem.* **1994**, *98*, 3459–3466.

explained by a structural transition from a surface-bound electron at smaller cluster sizes to a more solvated electron at the larger sizes: that is, an electron penetrating into the droplet. The larger RE value for $n = 60$ than for $n = 56$ is due to the increased electron solvation energy as a result of the electron being located more internally at the larger cluster size. The relatively sharp transition could be due to a critical minimum number of water molecules necessary to stabilize an internally solvated electron in these nanodrops containing a trivalent ion. In comparison to $La^{3+}(H_2O)_n$, the recombination enthalpy values for $Eu(H_2O)_n^{3+}$ decrease linearly and monotonically as a function of $n^{-1/3}$ from $n = 55$ to $n = 140$. The difference between the Eu^{3+} and La^{3+} data indicates that the nonlinearity at $n = \sim 58$ for La^{3+} is not due to a cluster-size-dependent phase transition.

The linear regression best fit of the $La(H_2O)_n^{3+}$ data for $n = 42-56$ results in a line with slope of 20 ± 2 eV, a *y*-axis intercept of $+0.3 \pm 0.5$ eV, and an R^2 value of 0.962; for the data with $n = 65-160$, linear regression results in a line with a slope of 17.5 ± 0.4 eV, a *y*-axis intercept of 1.34 ± 0.09 eV, and an R^2 value of 0.993. The *y*-axis intercept of the latter line corresponds to a value of -1.34 eV for the hydration enthalpy of the electron: that is, $e^-(g) \rightarrow e^-(aq)$. This value is well within the wide range of values obtained for the solvation enthalpy of the electron (-1.0 to -1.8 eV) from the reaction enthalpies for eqs 1,[18] 2,[19] and 3[20] and the values previously reported[26−33] for the solvation enthalpy of the proton. A more direct comparison of our value to those obtained from the pulse radiolysis data is complicated by the wide range of values for the proton solvation energy that have been reported. Our nanodrop extrapolation method to obtain the electron solvation enthalpy is entirely independent of the pulse radiolysis methods[18−20] and has the advantages that the proton and H atom solvation enthalpies do not need to be known.

To the extent that the electron is delocalized on the surface of smaller clusters ($n = 42-56$), the *y*-axis intercept of the best-fit line to these data corresponds roughly to a value of -0.3 ± 0.5 eV for the conduction band edge of liquid water, V_0: that is, the energy of forming a quasi-free delocalized electron in bulk water from the vacuum level with zero kinetic energy. The value for the conduction band edge of water has been the subject of some controversy with reported values as low as -1.3 eV[75] and a proposed upper limit as high as $+1.0$ eV.[76] More recent considerations suggest that the V_0 of liquid water is closer to zero.[30] The results from the nanocalorimetry data from $M(H_2O)_n$ ($M = Ca^{2+}$, La^{3+}; $V_0 \approx +0.6$[57] and -0.3 eV, respectively) bracket this estimated value of ~ 0 for the V_0 of liquid water[30] as well as a recently reported value of ~ 0 for ice.[43] Potential sources of uncertainty in these measurements are presented in the Supporting Information.

Conclusions

The fleetingly short lifetime of an electron in aqueous solution can obfuscate studies aimed at understanding electron hydration, whereas gaseous water clusters with an electron attached can be much longer lived, making possible characterization of electron hydration by a number of methods. However, the location of the electron in gaseous water clusters has been controversial, and evidence for up to three different structures has been reported.[34] Combining an electron with a gaseous water cluster containing a trivalent metal ion can result in either reduction of the metal ion or formation of a trivalent metal ion−electron pair in the overall reduced droplet. For La^{3+} clusters with between ~ 42 and 56 water molecules, capture of an electron results in formation of an ion−electron pair in which the electron is bound to the surface of the droplet, whereas capture by larger La^{3+}-containing droplets results in ion−electron pairs in which the electron is more internally solvated. By extrapolating the recombination energies obtained from the nanocalorimetry experiments on larger clusters to infinite cluster size, a value for the hydration enthalpy of an electron in bulk water of -1.34 eV with a precision of ± 0.09 eV is obtained. This method for establishing an electron solvation enthalpy has the advantages that the position of the electron in the larger droplet is more precisely known than for clusters that do not contain a metal ion, and there is no need for estimates of the solvation enthalpy of a proton or of atomic hydrogen.

The accuracy of these experiments could be significantly improved by experimentally calibrating the nanocalorimetry method using laser photodissociation experiments at multiple wavelengths, cluster sizes, and charge states. An increase in the magnetic field strength of the experimental apparatus from 2.75 to 7.0 T would make these experiments possible on clusters with up to about 900 water molecules, which would greatly improve the precision with which the electron solvation energy could be measured. These results clearly demonstrate that stabilization of ions by a finite number of water molecules can be substantial and even greater than the recombination energy of some trivalent metal ions with an electron. The results from these gas-phase electrochemical experiments correlate beautifully with traditional electrochemical experiments done in solution and provide a bridge between gas-phase and solution studies. An advantage of these measurements is that counterions can either be eliminated or precisely controlled by mass selection, which makes it more readily possible to measure ion effects directly. Such ion−electron recombination studies should ultimately lead to a better understanding of ion and electron stabilization in solution.

Acknowledgment. We thank the National Science Foundation (Grant No. CHE-0718790) for generous financial support and the Eastman Chemical Co. for sponsoring an ACS Division of Analytical Chemistry Summer Fellowship for W.A.D. Acknowledgment is made to the donors of the Petroleum Research Fund, administered by the American Chemical Society (No. 47916-AC6), for support of this research.

Supporting Information Available: Description of the relationship between $\langle d \rangle^{-1}$ and cluster size and sources of uncertainty. This material is available free of charge via the Internet at http://pubs.acs.org.

JA9079385

(75) Ballard, R. E. *Chem. Phys. Lett.* **1972**, *16*, 300–301.
(76) Jortner, J. *Ber. Bunsen-Ges. Phys. Chem.* **1971**, *75*, 696–714.